Supplementary Information

A. Theoretical model for dissolution of a drop in the MEFD – Governing Equations

In this section, we describe the governing equations and the boundary conditions used to determine the dissolution dynamics of a Hele-Shaw drop in the MEFD. Using the shallow channel approximation, we can solve for the linear extensional flow field as follows,

$$u = -\frac{b^2}{3\mu}\frac{\partial p}{\partial x} + b^2\left(\frac{\partial^2 u}{\partial x^2} + \frac{\partial^2 u}{\partial y^2}\right), \tag{1}$$

$$v = -\frac{b^2}{3\mu}\frac{\partial p}{\partial y} + b^2\left(\frac{\partial^2 v}{\partial x^2} + \frac{\partial^2 v}{\partial y^2}\right), \tag{2}$$

$$\frac{\partial u}{\partial x} + \frac{\partial v}{\partial y} = 0, \tag{3}$$

where, u and v represent the depth-averaged suspending fluid velocity, μ is the suspending fluid viscosity, b is the half-depth of the channel, p is the suspending fluid pressure field, and x and y are as shown in Figure SI 1a. The boundary conditions of the ambient field are, $u|_{r\to\infty} = Gx$, $v|_{r\to\infty} = -Gy$ and the interface stress condition, assuming a fully mobile interface, is given as, $\tau_{r\theta}|_{r=R} = 0$. For an immobile interface, the stress condition at the interface becomes, $u|_{r=R} = v|_{r=R} = 0$.

To solve for the concentration field, c, the solute (EtOAc in our experiments) balance equation is given as,

$$u\frac{\partial c}{\partial x} + v\frac{\partial c}{\partial y} = D\left(\frac{\partial^2 c}{\partial x^2} + \frac{\partial^2 c}{\partial y^2}\right), \tag{4}$$

and the boundary conditions for the far-field bulk concentration goes as $c|_{r\to\infty} = c_b$ and the interfacial concentration is given by $c|_{r=R} = c_s$. Figure SI 1a) shows the schematic of a drop dissolving in the MEFD.

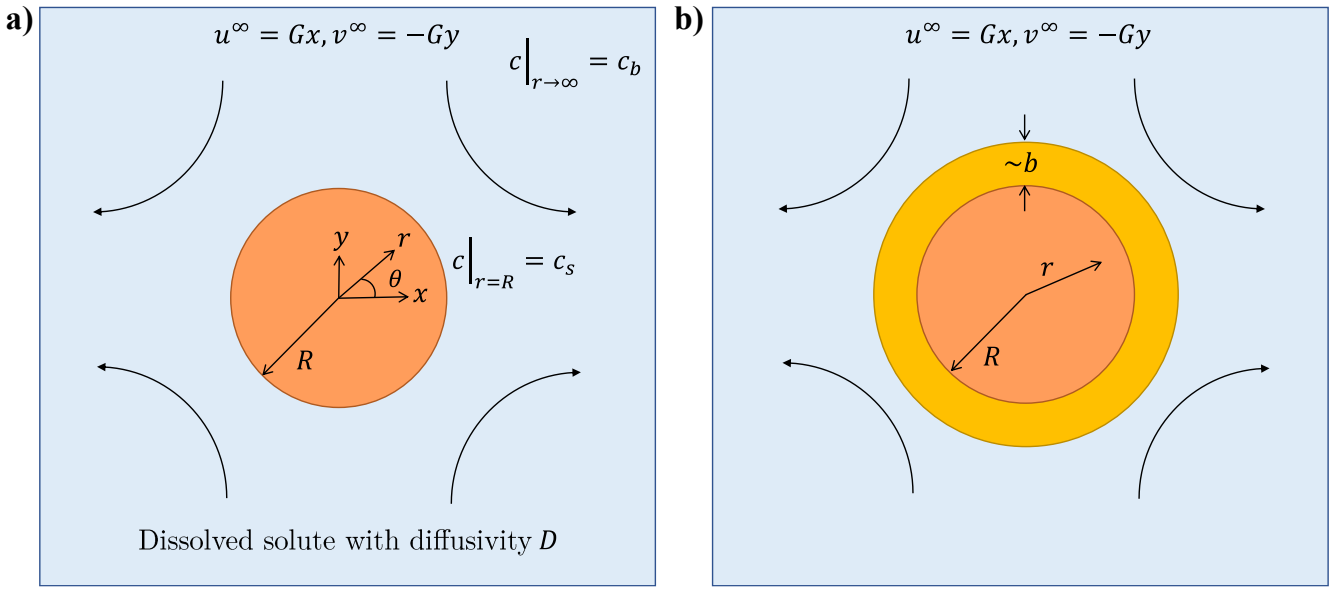

Figure SI 1. Theoretical model of drop dissolution in the MEFD: a) Schematic of the model of a dissolving EtOAc drop of radius R and diffusivity D in the suspending fluid (water). The solute solubility is c_s, whereas the bulk concentration is c_b; b) Schematic of boundary layer of thickness $\sim b$ and a secondary region of length $\sim R$ developing in the drop as the dissolution proceeds.

Going back to equation 1.4, $-\frac{dR}{dt} = k_{cw}\frac{(c_s - c_b)}{\rho_{EtOAc}}$, the mass transfer coefficient k_{cw} is the parameter of interest in this analysis. It is given as,

$$k_{cw}(c_s - c_b)\left(\frac{\pi}{2}\right)R = \int_0^{\pi/2} -D\frac{\partial c}{\partial r}\bigg|_{r=R} R d\theta, \tag{5}$$

and upon simplification reduces to,

$$k_{cw} = \frac{2}{(c_s - c_b)\pi}\int_0^{\pi/2} -D\frac{\partial c}{\partial r}\bigg|_{r=R} d\theta \tag{6}$$

As the dissolution proceeds, a boundary layer develops at the surface of the drop, as shown in Figure SI 1b). In the region of length scale $\sim R$, around the drop, the disturbance velocity decays as $(r/R)^{-3}$. However, in the region of thickness $\sim b$, the boundary condition on the surface of the drop affects the flow field. The mass transfer coefficient depends on the boundary layer thickness δ relative to the thickness of the inner region b, and whether or not the interface is mobile or immobile. The

Sherwood number Sh, given as $\mathrm{Sh} = k_{cw}R/D$, is a dimensionless mass transfer coefficient, and the Péclet number is given as $\mathrm{Pe} = GR^2/D$. If the interface is immobile, at high Pe, we expect a diffusive (in the normal direction to the interface) – convective (in the flow direction) balance of $\frac{\delta^2}{D} \sim \frac{R}{\frac{GR}{b}\delta}$, which gives us a boundary layer scaling as $\delta \sim \left(\frac{bD}{G}\right)^{\frac{1}{3}}$, and therefore the Sherwood number scaling as $\mathrm{Sh} \sim \mathrm{Pe}^{\frac{1}{3}}$ at constant b. If the interface is mobile, at high Pe, we expect a diffusive–convective balance of $\frac{\delta^2}{D} \sim \frac{R}{GR}$, which gives us a boundary layer scaling as $\delta \sim \left(\frac{D}{G}\right)^{\frac{1}{2}}$, and therefore the Sherwood number scaling as $\mathrm{Sh} \sim \mathrm{Pe}^{\frac{1}{2}}$.[1]

We can get the complete relationship of Sh with Pe over the entire range of Péclet numbers for mobile and immobile interfaces by simulation, as shown in figure SI 2. $\mathrm{Pe} >> 1$ shows the trends in the convection-dominated regime and $\mathrm{Pe} << 1$ represents the diffusion-dominated regime (Stokes' paradox).

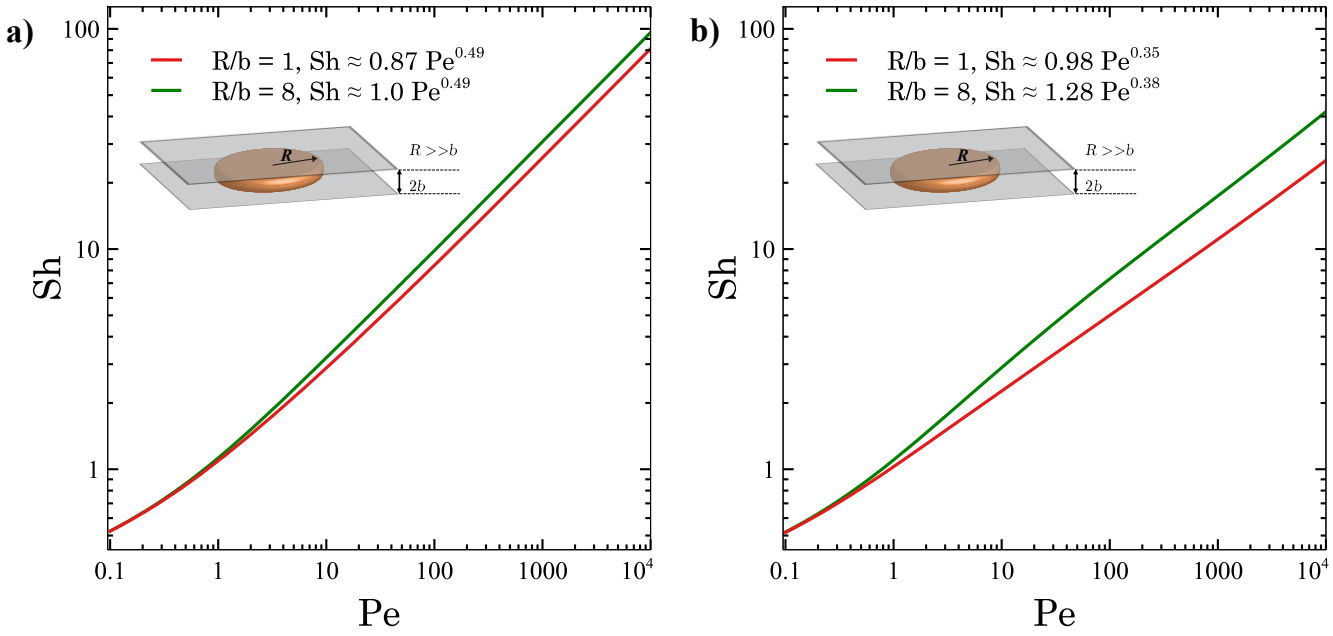

Figure SI 2. Relationship between Sherwood (Sh) and Péclet number (Pe): a) COMSOL simulation results for a fully mobile interface showing trends of $\mathrm{Sh} \sim \mathrm{Pe}^{1/2}$. The curves are a weak function of the aspect ratio R/b; b) A similar relationship between Sh and Pe calculated for an immobile interface

shows a larger dependence on the aspect ratio. For smaller aspect ratios, the behavior follows $\mathrm{Sh} \sim \mathrm{Pe}^{1/3}$.

In our experiments, we have observed that the interface is mobile. Figure SI 3) shows a drop with 3% PLGA dissolving in 2% PVA solution. We can see a droplet within the drop and as the drop is controlled and moved towards the stagnation point, the droplet moves along the interface. This gives us evidence to assume that the interface is mobile and use the appropriate scaling in our analysis. In this experiment, the stagnation point was slightly to the left of the center of the MEFD, and hence the drop is trapped slightly away from the center. Supplementary video 1a shows the dissolution of the drop shown here in Figure 3, and similarly, supplementary video 1b shows the dissolution of another 3% PLGA drop (not shown here).

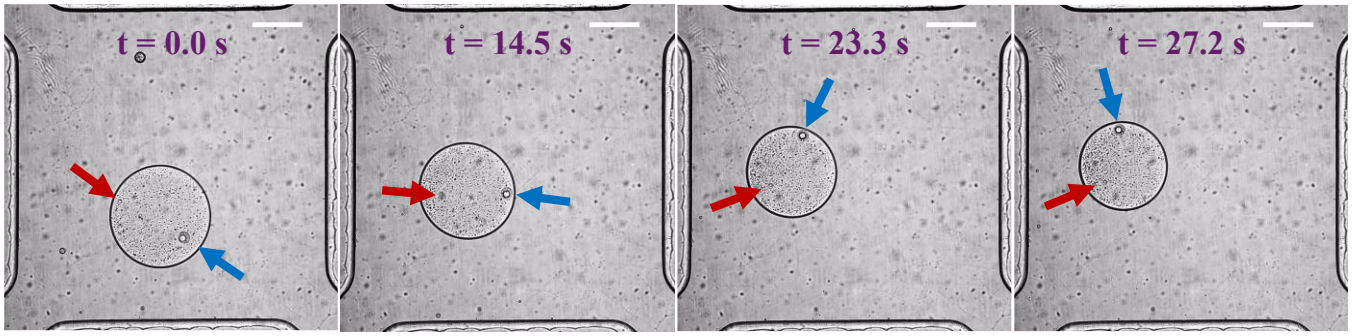

Figure SI 3. Observing mobile interface in the initial stages of dissolution: The images from left to right show a 3% PLGA drop in the MEFD. The blue and red arrows draw the reader's attention to the prominent droplets within the drop that move within the drop and along the interface indicating a mobile interface. The scale bar in each figure is 200 µm. Refer to supplementary video 1a to see the entire dissolution process of the drop, until the microparticle is lost to the extensional flow.

B. Mass transfer within the drop

The velocity inside the drop is related to the Hele-Shaw flow provided in the ambient. As the equation in velocity and pressure are linear, and since this flow is an extensional flow, the velocity on the interface must scale as $u_\theta \sim -GR \sin 2\theta$ in the first quadrant, provided the interface is mobile. Here, u_θ is the tangential velocity on the interface. In the COMSOL simulation, we applied a tangential velocity u_θ given by the above expression and computed the velocity field. The streamlines (Figure SI 4a.) show circulation, but only over a radial length is that is on the order of the depth of the channel; circulation in the interior of the channel is negligible ($R/b = 10$). This means that even if the Péclet number is high,

it will only cause fast mass transfer in the region close to the interface; the mass transfer over the interior of the drop will be diffusion-limited.

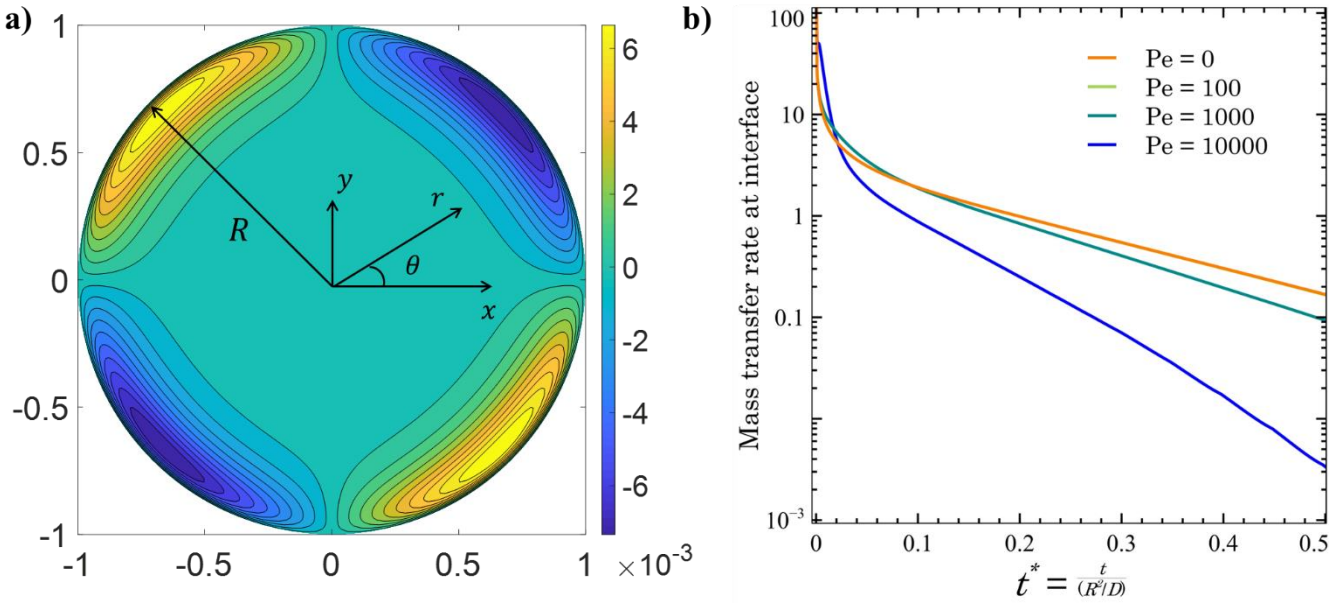

Figure SI 4. Simulation results for the mass transfer within the drop: a) COMSOL simulation result of the flow field inside the drop. There are circulation cells close to the interface, but they are weak in magnitude, and the central portion is still stagnant. Hence, we expect diffusion-dominated water transport in the drop with weak convective effects; b) Evolution of mass transfer rate into the drop with time for different Pe. The effect of the circulation on the concentration distribution becomes significant for Pe = 1000 or higher.

Additionally, we looked at the evolution of concentration with respect to time [Eq. 4]. The effect of the circulation on the concentration distribution becomes significant when Péclet numbers are closer to 1000 or larger. However, in our experiments, Pe values range from 1 – 100, in the initial stages of the extraction. Moreover, as the extraction proceeds, the viscosity of the drop phase increases, and circulation becomes progressively weaker. Hence, we expect the transport of water into the drop to be diffusion-dominated throughout the extraction process.

According to the main text, the Biot number Bi_m is order 1 or smaller during the initial stages. Hence, the mass transfer that matters is the one in the suspending phase, and not in the drop phase. But the slow phase in Figure 5b) at later times is due to the diffusive process inside the drop phase. This diffusion, and the phenomenon of curing, are left for future work.

C. Extraction studies with 12 wt% PLGA drop

To study the effect of higher polymer concentration in the drop, we conducted experiments with 12% PLGA in the drop, and Figure SI 5 (and Supplementary Video 5) shows the dissolution trend of one such drop. We observed that the drop dissolved linearly with time in the initial stages, and in the later stages showed a constant R behavior. This trend was consistent with our observations made for a 3% PLGA drop. However, the transition between dR/dt = constant and the R = constant behavior is elongated in the 12% PLGA drop as opposed to the 3% drop (Fig. 5b in the main text). This is so because the 12% polymer drop reached the denser and more viscous state faster than the 3% drop, due to the lower concentration of solvent in the 12% drop. This possibly leads to two things: first, the density in the denominator of the right-hand side (Eq. 1.4, main text) is not ρ_{EtOAc} , but ρ_{mix}, the combined density of PLGA and EtOAc, which could be happening initially in the transient state too. Second, the mass transfer rate inside the drop is gaining prominence compared to the external mass transfer rate. Both these observations apply to a 3% PLGA drop as well, only the behavior is more enhanced with the 12% PLGA experiment. On a separate note, it was more challenging to conduct experiments with higher polymer concentrations in the MEFD, due to undue gelation of polymer solution stream/drops near the T-junction. One possible way to reduce this effect could be by partially saturating the suspending medium with the solvent (EtOAc) to reduce the rate of extraction, as predicted by the relationship $\frac{dR}{dt} \approx -\frac{(DG)^{1/2}(c_s - c_b)}{\rho_{EtOAc}}$ (equation 1.10 in the main text). This is left for future investigation.

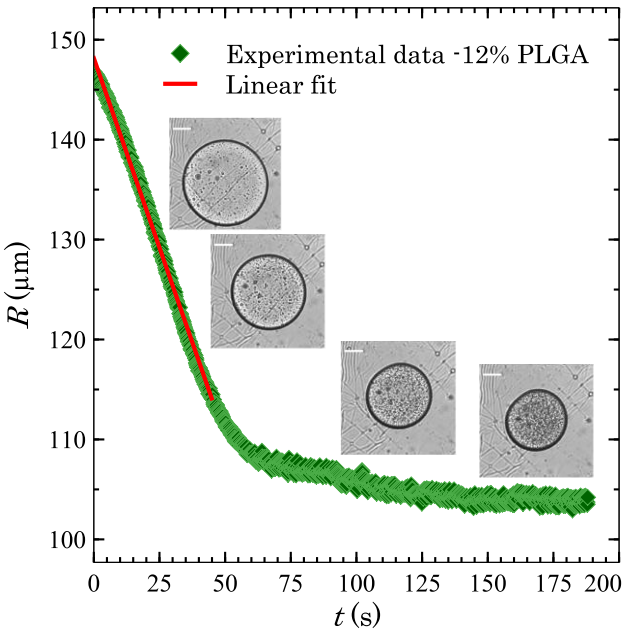

Figure SI 5. Observations with higher polymer concentration in the drop: Dissolution trend for a 12% PLGA drop dissolving in 2% PVA solution at $G = 0.41\ s^{-1}$ and the linear regime of solvent extraction follows $R = -0.76t + 148$. The insets show the dissolution of the drop and the subsequent formation of the polymer microparticle. The dissolution in the later stage (after around 45 s) changes slope and gradually slows down as a microparticle of nearly constant size is formed. The scale bar in the insets is 45 μm.

D. Dissolution trends of a single EtOAc and PLGA drop at $G \sim 1\ s^{-1}$

Figure SI 6 shows the dissolution trends of an EtOAc drop at $G = 0.8\ s^{-1}$ and a 3% PLGA drop at $G = 0.85\ s^{-1}$, to present another example of the dissolution trends at a higher strain rate (~ $1\ s^{-1}$).

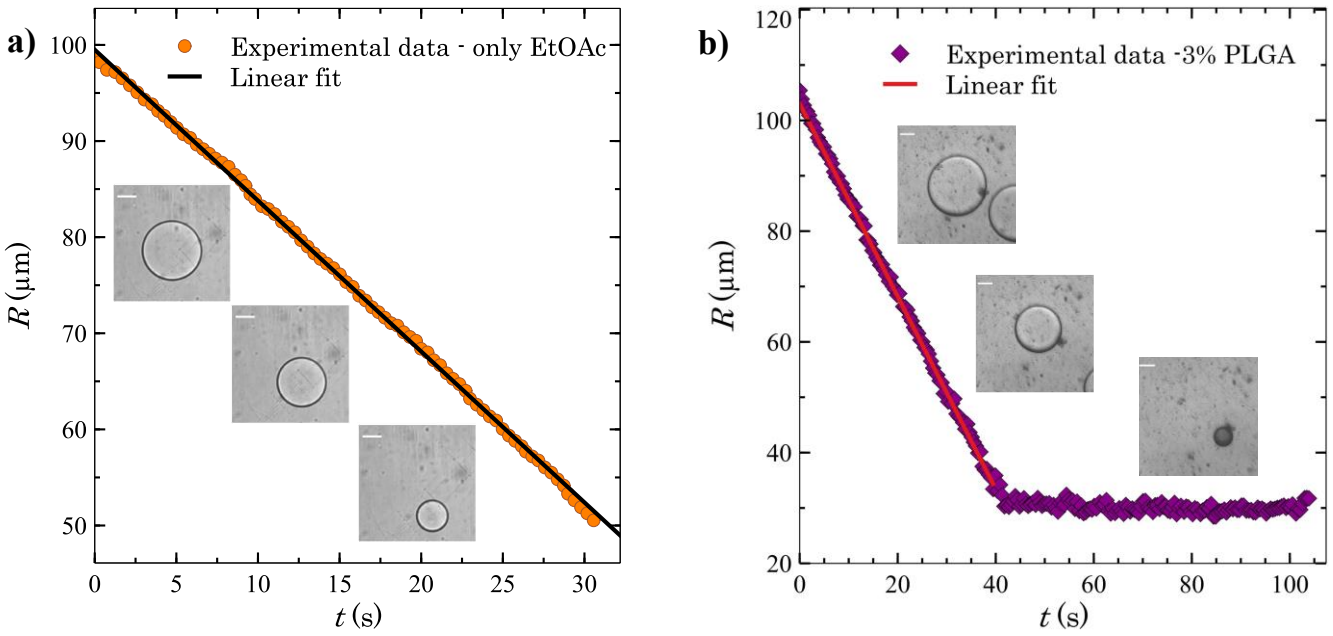

Figure SI 6. Dissolution trends of a single drop in the MEFD: a) Dissolution trend (alternatively extraction trend) for an EtOAc drop dissolving in 2% PVA solution at $G = 0.8\ s^{-1}$. The linear part of the dissolution curve is given by $R = -1.6\,t + 99$; b) Dissolution trend for a 3% PLGA drop dissolving in 2% PVA solution at $G = 0.85\ s^{-1}$ and the linear regime of solvent extraction follows $R = -1.7\,t + 103$. The scale bar in the insets is 45 μm.

Description of Supplementary Videos

Supplementary Video 1. Mobile interface in a dissolving PLGA-EtOAc drop: a) A 3% PLGA drop to show that the interface is mobile, at least during the initial phase of the dissolution. The viewer's attention is directed to the droplets inside the drop, as marked in Figure SI 3. The stagnation point in this experiment was slightly off the center of the device, and hence the drop is trapped slightly skewed to the left of the center; b) Another 3% PLGA drop to show the mobile interface. The videos are playing at 1.5x speed. The scale bar is 200 μm.

Supplementary Video 2. Trapping of a drop in the MEFD using an analytical solution of the flow field: The video shows the control of a 3% PLGA using a computer-feedback-driven algorithm. The flow rates in the MEFD are adjusted to bring the drop to the stagnation point of the device where it is hydrodynamically trapped and observed. Once the drop becomes smaller than the channel depth ($2b = 100\ \mu m$ in all our experiments), the drop no longer satisfies the Hele-Shaw requirement of $R >> b$, and hence it becomes hard to trap the drop. The drop/microparticle is usually lost to the extensional flow at this stage. The dissolution process is continuously captured and later processed to obtain the dissolution rate. The video is playing at 1.5x speed. The scale bar is 200 μm.

Supplementary Video 3: Dissolution of an EtOAc drop in 2% PVA solution: An EtOAc drop dissolving linearly with time in 2% PVA solution, until the drop becomes much smaller than the channel half-depth and is lost to the extensional flow. The scale bar is 45 μm.

Supplementary Video 4: Dissolution of a 3% PLGA drop in 2% PVA solution: An EtOAc drop with 3 wt% PLGA, dissolving in 2% PVA solution to form a polymer microparticle of constant radius. The initial stage of dissolution is linear with time, followed by the change in slope as the bulk of the solvent has been extracted from the drop. The scale bar is 45 μm.

Supplementary Video 5: Dissolution of a 12% PLGA drop in 2% PVA solution: The drop dissolves linearly with time in the initial stage of dissolution, just as seen in a 3% PLGA drop followed by a more gradual change of slope before the drop loses most of the solvent and the polymer microparticle is formed. The scale bar is 45 μm.

References

1. Goel, S. The Roles of Dissolution, Coalescence, and Interfacial Tension in the Formation and Stability of Extremely Fine Water Drops in Concentrated Bitumen Solutions. (2019).